Tm 3+ and Ho 3+ colasing in in-band pumped waveguides fabricated by femtosecond laser writing

Esrom Kifle, Pavel Loiko, Carolina Romero, Javier Rodríguez Vázquez de Aldana, Viktor Zakharov, Yulia Gurova, Andrey Veniaminov, Valentin Petrov, Uwe Griebner, Romain Thouroude, et al.

Tm^{3+} and Ho^{3+} colasing in in-band pumped waveguides fabricated by femtosecond laser writing

Esrom Kifle,[1,2] Pavel Loiko,[2] Carolina Romero,[3] Javier Rodríguez Vázquez de Aldana,[3] Viktor Zakharov,[4] Yulia Gurova,[4] Andrey Veniaminov,[4] Valentin Petrov,[5] Uwe Griebner,[5] Romain Thouroude,[2] Mathieu Laroche,[2] Magdalena Aguiló,[1] Francesc Díaz,[1] Patrice Camy,[2] and Xavier Mateos[1,*]

[1]Universitat Rovira i Virgili (URV), Física i Cristal·lografia de Materials i Nanomaterials (FiCMA-FiCNA), Marcel.li Domingo 1, 43007 Tarragona, Spain
[2]Centre de Recherche sur les Ions, les Matériaux et la Photonique (CIMAP), UMR 6252 CEA-CNRS-ENSICAEN, Université de Caen Normandie, 6 Boulevard du Maréchal Juin, 14050 Caen Cedex 4, France
[3]Aplicaciones del Láser y Fotónica, University of Salamanca, 37008 Salamanca, Spain
[4]ITMO University, 49 Kronverkskiy Pr., 197101 St. Petersburg, Russia
[5]Max-Born-Institute for Nonlinear Optics and Short-Pulse Spectroscopy, 2A Max-Born-Str., D-12489 Berlin, Germany
**Corresponding author: xavier.mateos@urv.cat*

Received XX Month XXXX; revised XX Month, XXXX; accepted XX Month XXXX; posted XX Month XXXX (Doc. ID XXXXX); published XX Month XXXX

We report on the first in-band pumped Tm^{3+},Ho^{3+} codoped waveguide (WG) laser. A depressed-index surface channel WG (type III) with a 50 μm half-ring cladding is fabricated in a 5 at.% Tm^{3+}, 0.5 at.% Ho^{3+}:$KLu(WO_4)_2$ crystal by femtosecond pulse direct laser writing. Under in-band pumping by a 1679-nm Er Raman fiber laser, Tm^{3+} and Ho^{3+} colasing is observed in the WG and explained by bidirectional energy transfer. The maximum total output power at ~1942 nm (Tm^{3+}) and 2059 nm (Ho^{3+}) is 448 mW with a slope efficiency of 40.6%, record-high for this type of WG lasers. The maximum output power of the Ho-laser reaches 144 mW. © 2020 Optical Society of America

http://dx.doi.org/10.1364/OL.99.099999

The Holmium ion (Ho^{3+}) is attractive for solid-state laser emission at wavelengths slightly above 2 μm ($^5I_7 \rightarrow {}^5I_8$ transition), falling in the eye-safe spectral range. Holmium lasers are of practical interest for remote sensing, wind mapping, medicine and further frequency conversion into the mid-IR. A common way to excite the Ho^{3+} ions is codoping of the host matrix with thulium (Tm^{3+}) ions acting as sensitizers [1,2]. Tm^{3+} ions can be pumped at ~0.8 μm (to the $^3H_4$ state) transfering a part of the energy of the electronic excitation to the Ho^{3+} ones via non-radiative energy-transfer (ET), $Tm^{3+}(^3F_4) \rightarrow Ho^{3+}(^5I_7)$ [3] and such codoped *bulk* laser can be very efficient [1]. A diode-pumped Tm,Ho:$KLu(WO_4)_2$ (Tm,Ho:KLuW) laser generated an output power of 451 mW at 2081 nm with a slope efficiency of 31% [2]. Tm^{3+},Ho^{3+} codoped materials are also attractive for mode-locked lasers at >2 μm [4,5]. Their emission wavelength is red-shifted (with respect to singly Tm^{3+} doping) avoiding the structured water vapor absorption and the combined gain bandwidth is broader favoring sub-100 fs pulses [4,5].

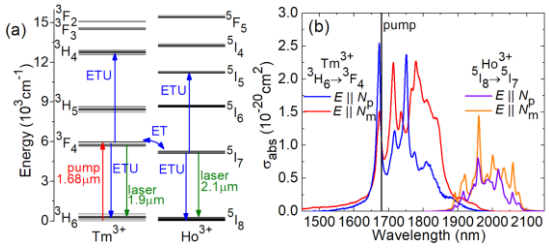

Fig. 1. In-band pumping of Tm,Ho:KLuW: (a) energy-level scheme of Tm^{3+} and Ho^{3+}: *red (green) arrow* – pump (laser) transition, ET – energy-transfer, ETU – energy-transfer upconversion; (b) absorption cross-sections, σ_{abs}, for the $^3H_6 \rightarrow {}^3F_4$ Tm^{3+} and $^5I_8 \rightarrow {}^5I_7$ Ho^{3+} transitions and light polarized along the N_p and N_m optical indicatrix axes.

Optically "passive" surface waveguides (WGs) supporting light guiding at ~2 μm could find applications in bio- and environmental sensing based on evanescent-field interaction with material on the surface. The probing of "passive" WGs can be provided by another integrated ("active") device. "Active" surface WGs are also suitable for pulsed sources based on interaction with a surface-deposited saturable absorber [6]. Efficient surface Tm^{3+},Ho^{3+} WG lasers with a broadband emission around 2 μm are excellent candidates for these

aims. Unfortunately, so far, only few studies have been devoted to this topic [7-9]. Planar Tm^{3+},Ho^{3+} codoped WGs based on $KY(WO_4)_2$ and $LiYF_4$ layers grown by Liquid Phase Epitaxy (LPE) are known [7,8]. A Tm,Ho:$LiYF_4$ planar WG laser generated 81 mW at 2051 nm with a slope efficiency of 24% [8]. In [9], buried channel WGs were fabricated in bulk Tm,Ho:ZBLAN glass by femtosecond Direct Laser Writing (fs-DLW) yielding 76 mW at 2052 nm with a similar slope. Note that in all of these publications, the conventional pump scheme (excitation to the $^3H_4$ level of Tm^{3+}) was used.

The difficulty in developing Tm^{3+},Ho^{3+} lasers in general, and such WGs in particular, is the strong thermal effect [2] due to energy losses occurring in the following processes: relaxation of Tm^{3+} ions to the $^3F_4$ state, possible $Ho^{3+} \rightarrow Tm^{3+}$ back ET and energy-transfer upconversion (ETU) for both ions. In part, it can be alleviated by direct (in-band) pumping of Tm^{3+} to the $^3F_4$ state, Fig. 1(a). *Bulk* in-band pumped Tm^{3+},Ho^{3+} lasers are known [10]. Recently, we reported the first singly Tm-doped in-band pumped channel WG laser delivering up to 2.05 W at 1881 nm with a record-high slope efficiency of 78.3% [11]. In the present work, we demonstrate the first in-band pumped Tm^{3+},Ho^{3+} codoped WG laser.

As a gain material, we employed monoclinic (sp. gr. $C2/c$) 5 at.% Tm, 0.5 at.% Ho:KLuW grown by the top seeded solution growth method using $K_2W_2O_7$ as a solvent. The actual Tm^{3+} and Ho^{3+} doping levels were determined by electron probe microanalysis to be N_{Tm} = 2.30×10^{20} cm^{-3} and N_{Ho} = 0.53×10^{20} cm^{-3}. A rectangular sample was cut in the frame of the optical indicatrix of KLuW which is an optically biaxial crystal. The uncoated sample was 3.0-mm thick along the N_g-axis. Its 5.8(N_m)×1.5(N_p) mm^2 input and output faces (pump and laser propagation) and the top surface were polished.

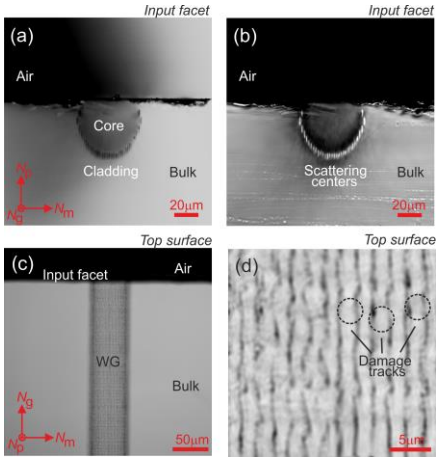

Fig. 2. Confocal microscopy study of the fs-DLW Tm^{3+},Ho^{3+} codoped surface channel WGs in Tm,Ho:KLuW: (a,b) end-facet view - (a) bright and (b) dark field; (c,d) top surface view in bright field: (c) area adjacent to the input facet, (d) individual damage tracks. Transmission mode, polarized light P: (a,b) P || N_p, (c,d) P || N_g. λ = 405 nm.

Depressed-index guides with a half-ring cladding (type III) were fabricated by fs-DLW. To produce individual damage tracks, the output of a Ti:Sapphire regenerative amplifier (Spitfire, Spectra Physics) delivering 120 fs (795 nm central wavelength) at 1 kHz repetition rate was focused into the bulk volume of the material through the top surface (N_m×N_g). Only a small fraction of the pulse energy was employed (65 nJ). The writing optics comprised a 40× microscope objective (numerical aperture: N.A. = 0.65). The crystal was scanned at a speed of 500 μm/s along its N_g-axis resulting in the formation of the damage tracks. The polarization of the fs laser was perpendicular to the writing direction ($\boldsymbol{E}$ || N_m). No repolishing after the inscription of the damage tracks was applied.

The geometry of the guides was inspected using a confocal laser microscope (LSM 710, Carl Zeiss). The resolution was 0.24 μm. The end-facet view with polarized light (P || N_p) in bright field, Fig. 2(a), reveals a half-ring cladding formed by 31 vertically elongated (direction of the laser propagation) damage tracks. The diameter of the cladding is ~50 μm and the upper / lower tracks are located at 12 / 49 μm beneath the crystal surface. The cross-section size of each track is 1(horizontal, N_m) × 6(vertical, N_p) μm^2 and their separation is 2 μm (horizontal). No macroscopic cracks in the core or in the surrounding bulk area are observed. The inspection of the same area in dark field, Fig. 2(b), reveals bright scattering centers coinciding with the written tracks. The top view with polarized light (P || N_g), Fig. 2(c), indicates that the damage tracks are continuous, and they propagate through the entire length of the sample reaching the end-facets at both sides. The cladding resembles a canvas-like structure. Individual tracks are visualized in Fig. 2(d) showing dark borders and a brighter inner part probably due to local expansion and partial amorphization of the material subjected to the fs temporal structure of the pulses.

To study the effect of the fs laser writing irradiation on the emission properties of rare-earth ions (Tm^{3+} and Ho^{3+}), the intensity of the green Ho^{3+} emission was monitored across the end-facet area, Fig. 3(a). It revealed a clear drop in the emission intensity within the cladding and almost unchanged luminescence response of the core. A close look on the individual damage tracks from the top surface, Fig. 3(b), indicated a strong localization of the depressed emission intensity within the dark "sidewalls" of the tracks.

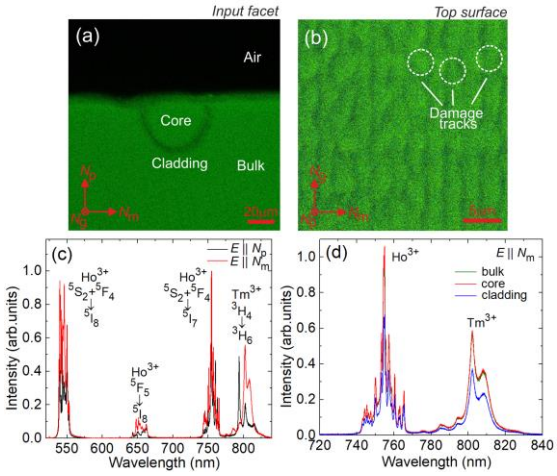

Fig. 3. μ-luminescence study of the fs-DLW Tm^{3+},Ho^{3+} codoped surface channel WGs: (a,b) μ -luminescence mapping: (a) end-facet view, (b) top view, a closer look on the damage tracks. $^5S_2$+$^5F_4$ → $^5I_8$ Ho^{3+} emission, unpolarized light; (c) polarized emission spectra from the core region for light polarizations $\boldsymbol{E}$ || N_p and $\boldsymbol{E}$ || N_m; (d) comparison of the emission spectra from Ho^{3+} and Tm^{3+} ions from the bulk, core and cladding regions of the WG, $\boldsymbol{E}$ || N_p. The excitation wavelength λ_{exc} is 488 nm.

Using a confocal Raman microscope, (InVia, Renishaw) equipped with a 50× objective, we measured the micro-luminescence spectra

from the core region for $\boldsymbol{E} \parallel N_p$ and $\boldsymbol{E} \parallel N_m$, Fig. 3(c). This confirmed well-preserved strong anisotropy of the spectroscopic properties of the material in the core region. By focusing of the 488 nm radiation on three areas (focus diameter: 2 μm) in the surrounding bulk material, in the WG core and on the WG cladding, we compared the emission spectra of Ho^{3+} ($^5S_2+^5F_4 \rightarrow {}^5I_7$ transition) and Tm^{3+} ($^3H_4 \rightarrow {}^3H_6$ transition) ions. As shown in Fig. 3(d), there is no reduction in intensity nor alteration of the spectral shape for the core region. The emission intensity is depressed in the cladding, in agreement with Fig. 3(a), while only slight changes in the spectral shape (e.g., peak shifts and broadening) are detected in our study. It suggests a slight and strongly spatially localized alteration of the crystal field around the rare-earth ions.

The laser experiments were performed in a linear plano-plano laser cavity containing a pump mirror (PM) coated for high transmission at the pump wavelength (HT, T = 93% at 1.68 μm) and for high reflection (HR) at 1.87-2.30 μm, and a set of output couplers (OCs) with an actual transmission at the laser wavelength T_{OC} in the range of 1.5%...20%. OCs with higher transmissions (T_{OC} = 30%-50%) resulted only in Tm^{3+} lasing with deteriorated performance and, thus, they were not studied. Both cavity mirrors were gently pressed towards the crystal end-facets (without any index-matching liquid) leading to a geometrical cavity length of 3.0 mm. The sample was fixed on a Cu-holder using a silver paint.

The pump source was a home-made Raman fiber laser (RFL) [11]. It comprised of a 1560 nm Erbium Master-Oscillator Power Amplifier (MOPA) and a polarization-maintaining GeO_2-doped silica fiber with a Raman-active mode at ~440 cm^{-1}. The RFL delivered 4.0 W at 1679 nm (emission bandwidth: 1 nm), linearly polarized and a spatially single-mode output (M^2 <1.1). The pump wavelength corresponded to the $^3H_6 \rightarrow {}^3F_4$ Tm^{3+} transition (in-band pumping), Fig. 1(b). The pump was focused through the PM using a spherical uncoated CaF_2 lens (f = 40 mm, T = 94%). The measured pump spot diameter at the input WG facet $2w_P$ was 30±5 μm. The pump polarization corresponded to $\boldsymbol{E} \parallel N_m$. More details about the laser set-up can be found elsewhere [11].

The pump coupling efficiency $\eta_{coupl} = P_{coupl}/P_{inc} \approx 89\%$ was simply estimated from Fresnel losses (refractive index n_m = 2.002), because the pump spot size is smaller than the WG dimensions and the condition $(N.A.)_{pump} < (N.A)_{WG} \approx 0.05$ was satisfied. The absorption under non-lasing conditions, $\eta_{abs,NL} = P_{abs}/P_{coupl}$, was determined from measurements of the transmitted pump. A strong absorption bleaching was detected: $\eta_{abs,NL}$ gradually decreased below its small-signal value, $\eta_{abs,0} = 1 - \exp(-\sigma_{abs}^P N_{Tm} t) = 50.9\%$, where $\sigma_{abs}^P = 1.03\times10^{-20}$ cm^2 and t = 3.0 mm, Fig. 1(b). The small-signal single-pass pump absorption length was 4.2 mm. The absorption under lasing conditions, $\eta_{abs,L}$, was calculated from the $\eta_{abs,NL}$ value at the threshold pump power for each OC accounting for the double-pass of the pump because the OCs were highly-reflective at ~1.68 μm. The $\eta_{abs,L}$ value obtained, in the range 42 – 49±1% (depending on the OC) ensured almost uniform pumping (inversion) in the WG [8].

The output beam was collimated with an uncoated CaF_2 lens (f = 15 mm) and a cut-off filter (T < 0.001% at ~1.68 μm) was used to filter out the residual pump. An optical spectrum analyzer (OSA, AQ6375B, Yokogawa) equipped with a multimode low-OH optical fiber served for recording the emission spectra. The laser beam profile was captured using a FIND-R-SCOPE near-IR camera; the scale was calibrated by illuminating WGs with a known size.

The output dependences of the Tm,Ho WG laser are shown in Fig. 4(a). For all the studied output couplers, colasing of Tm^{3+} ($^3F_4 \rightarrow {}^3H_6$ transition) and Ho^{3+} ($^5I_7 \rightarrow {}^5I_8$ transition) ions was observed. Thus, we first measured the total (Σ = Tm+Ho) power. The maximum power was 448 mW at ~1942 nm (Tm^{3+}) and 2059 nm (Ho^{3+}) with a slope efficiency η_Σ of 40.6% (vs. P_{abs}) (T_{OC} = 9%). The laser threshold occurred at P_{abs} = 334 mW and the optical-to-optical efficiency $\eta_{opt\Sigma}$ was 28.2% (vs. P_{inc}). The laser threshold increased with T_{OC}, from P_{abs} = 120 mW (T_{OC} = 1.5%) to 366 mW (T_{OC} = 20%).

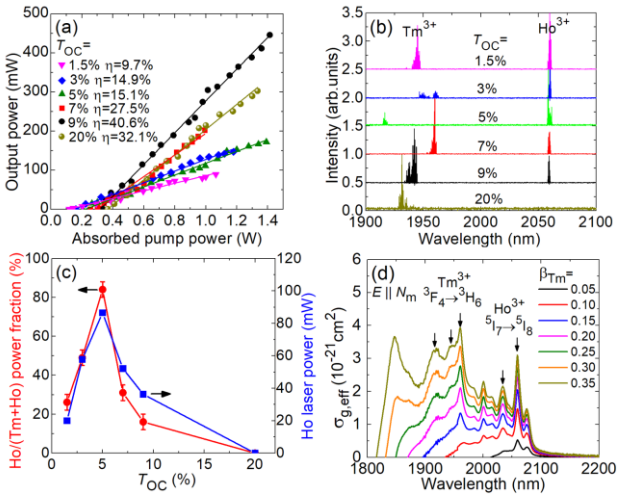

Fig. 4. CW in-band pumped Tm^{3+},Ho^{3+} codoped surface channel WG laser: (a) input-output dependences, η – slope efficiency; (b) emission spectra, P_{abs} = 0.9 W; (c) relative power fraction of Ho^{3+} emission, Ho/(Tm+Ho), and the Ho^{3+} output power *vs.* output coupling, P_{abs} = 0.9 W; (d) Effective gain cross-sections, $\sigma_{g,eff}$, for different Tm^{3+} inversion ratios $\beta_{Tm} = N_2(^3F_4)/N_{Tm}$, *arrows* indicate the observed laser wavelengths. The laser polarization is $\boldsymbol{E} \parallel N_m$.

The laser emission for the studied OCs was linearly polarized ($\boldsymbol{E} \parallel N_m$, horizontal) and the polarization state was naturally selected by the gain anisotropy for both Tm^{3+} and Ho^{3+} transitions. Typical spectra are shown in Fig. 4(b). The Ho^{3+} laser wavelength (~2059 nm) was almost independent on T_{OC}; the Tm^{3+} emission occurred between 1915 - 1963 nm, showing a tendency for a blue-shift with increasing the T_{OC} due to the quasi-three-level Tm laser scheme with reabsorption. The assignment of the emissions is according to the gain spectra of Tm^{3+} and Ho^{3+} ions for $\boldsymbol{E} \parallel N_m$.

The wavelength difference for Tm^{3+} and Ho^{3+} allowed separating the corresponding power fractions using a dichroic mirror, e.g., that for Ho^{3+} part: Ho/(Ho+Tm), Fig. 4(c). Both the Ho^{3+} power fraction, Ho/(Ho+Tm), and the output power, $P_{out,Ho}$, showed a complex dependence on the output coupling. The maxima for both these parameters ocurred at the same intermediate T_{OC} = 5% (for which the fraction Ho/(Ho+Tm) = 84±4%). For higher T_{OC}, both parameters gradually decrease to zero (for T_{OC} = 20%, Ho/(Ho+Tm) < 1%). Thus, the maximum Ho^{3+} output power is observed for T_{OC} = 5% amounting to 144 mW. Note that for this output coupler, the total (Tm+Ho) characteristics are: 174 mW at 1916 nm (Tm^{3+}) and 2059 nm (Ho^{3+}) with η_Σ = 15.1% and a laser threshold of 206 mW. The minimized Tm power fraction for this OC corresponding to a wavelength of 1916 nm can explain this blue-shift of the Tm^{3+} emission.

The example power dependence of the Tm^{3+} and Ho^{3+} WG laser is illustrated in Fig. 5 for T_{OC} = 3%. Note the slightly nonlinear

dependence explained by a power redistribution between Tm^{3+} and Ho^{3+} lasing. The threshold is much lower for the Ho^{3+} laser (161 mW) than for Tm^{3+} (320 mW). The Ho^{3+} power first increases linearly with a slope efficiency η_{Ho} of 15.9%. As soon as the threshold for Tm^{3+} lasing is reached, its power increases nonlinearly at the expense of the Ho^{3+} one. The corresponding slope efficiency η_{Tm} is 15.3%, obtained by fitting the output dependence well above the Tm^{3+} laser threshold. The laser spectra, Fig. 5(b), broaden with increasing the pump power very pronounced for the Tm emission.

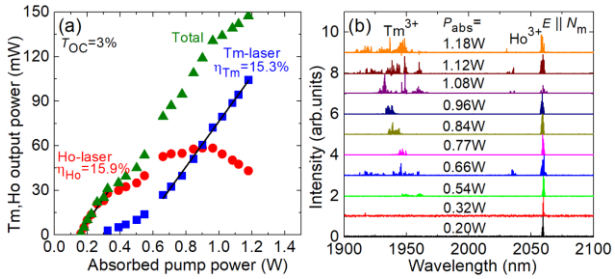

Fig. 5. Power and spectral properties of Tm^{3+} and Ho^{3+} emissions from the in-band pumped Tm^{3+},Ho^{3+} codoped surface channel WG laser: (a) input-output dependences (total and individual Tm and Ho lasing), $\eta_{Tm(Ho)}$ – slope efficiency for Tm^{3+}- and Ho^{3+}-lasing, respectively; (b) laser emission spectra versus P_{abs}. The laser polarization is $\boldsymbol{E} \parallel N_m$.

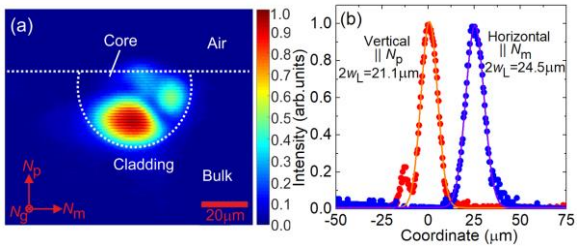

Fig. 6. Near-field intensity profile of the Ho lasing mode of the in-band pumped Tm^{3+}, Ho^{3+} codoped surface channel WG laser: (a) 2D mode profile, dashed lines indicate the crystal / air interface and the WG cladding; (b) 1D intensity plots along the horizontal ($\parallel N_m$) and vertical ($\parallel N_p$) directions, *symbols* – experimental data, *curves* - Gaussian fits. The laser polarization, $\boldsymbol{E} \parallel N_m$, is horizontal. T_{OC} = 5%, P_{abs} = 1.0 W.

The Tm^{3+} and Ho^{3+} emission channels both produced a spatially multimode output. The beam profiles were almost identical. The typical near-field profile of the Ho-laser captured using the near-IR camera and a dichroic mirror to eliminate Tm emission is shown in Fig. 6(a). More than 75% of the power was contained in the main lobe. It had an asymmetric shape extended along the horizontal direction ($\parallel N_m$) and it was localized not symmetrically with respect to the WG cladding, adjacent to its bottom. The lobe had nearly Gaussian intensity profiles in the horizontal and vertical directions, Fig. 6(b), corresponding to the mode diameters (at the $1/e^2$ level) $2w_L$ of 24.5 μm ($\parallel N_m$) and 21.1 μm ($\parallel N_p$). The mode was well localized within the WG cladding.

To explain the observed colasing, we calculated the effective gain cross-sections, $\sigma_{g,eff}$, for the Tm^{3+},Ho^{3+}-codoped KLuW crystal:

$$\sigma_{g,eff} = \sigma_{g,Ho}\left(N_{Ho}/N_{\Sigma}\right) + \sigma_{g,Tm}\left(N_{Tm}/N_{\Sigma}\right), \quad \textbf{(1a)}$$

$$\sigma_{g,Tm(Ho)} = \beta_{Tm(Ho)}\sigma_{SE,Tm(Ho)} - (1-\beta_{Tm(Ho)})\sigma_{abs,Tm(Ho)}, \quad \textbf{(1b)}$$

Here, $\beta_{Tm} = N_2(^3F_4)/N_{Tm}$ and $\beta_{Ho} = N_7(^5I_7)/N_{Ho}$ are the inversion levels for Tm^{3+} and Ho^{3+} ions, respectively, σ_{SE} and σ_{abs} are the stimulated-emission and absorption cross-sections, respectively, for both the $^3F_4 \leftrightarrow {}^3H_6$ Tm^{3+} and $^5I_7 \leftrightarrow {}^5I_8$ Ho^{3+} transitions, and $N_{\Sigma} = N_{Tm} + N_{Ho}$. The relation between β_{Tm} and β_{Ho} was determined accounting for the parameters of the bidirectional $Tm^{3+} \leftrightarrow Ho^{3+}$ ET [3] in Tm,Ho:KLuW, P_{28} = 1.69×10^{-22} $cm^3\mu s^{-1}$ (direct ET) and P_{71} = 0.15×10^{-22} $cm^3\mu s^{-1}$ (back ET) [12]. For low β_{Tm} <0.20, typical for bulk Tm^{3+},Ho^{3+} lasers, the local peaks at 2075 and 2059 nm are assigned to Ho^{3+} emission. These peaks are most pronounced in the gain spectra. For higher inversion levels (β_{Tm} and, accordingly, β_{Ho}), the peaks at 1915, 1946 and 1960 nm (Tm^{3+}) and at 2034 and 2059 nm (Ho^{3+}) dominate and correspond to close gain leading to Tm^{3+},Ho^{3+} colasing.

To conclude, the combination of fs-DLW to fabricate surface channel WGs in anisotropic crystals and in-band pumping by a Raman fiber laser to alleviate thermal issues is a novel approach for the development of integrated light sources emitting at ~2 μm. We report on a record-high Ho^{3+} output from a Tm^{3+},Ho^{3+} codoped WG laser. Single Ho^{3+} emission will be possible at lower propagation losses (lower β) and lower Ho/Tm ratios.

Funding. Spanish Government, MINECO (MAT2016-75716-C2-1-R (AEI/FEDER,UE), FIS2017-87970-R); Generalitat de Catalunya (2017SGR755); Junta de Castilla y León (SA287P18); Ministry of Science and Higher Education of Russian Federation (Goszadanie 2019-1080); Agence Nationale de la Recherche (LABEX-EMC3); European Union (European Regional Development Fund, ERDF); Regional Council of Normandie (NovaMat).

Disclosures. The authors declare no conflicts of interest.

References

1. G. L. Bourdet and G. Lescroart, Appl. Opt. **38**, 3275 (1999).
2. P. Loiko, J. M. Serres, X. Mateos, K. Yumashev, N. Kuleshov, V. Petrov, U. Griebner, M. Aguiló, and F. Díaz, Opt. Express **22**, 27976 (2014).
3. B. M. Walsh, N. P. Barnes, and B. Di Bartolo, J. Lumin. **90**, 39 (2000).
4. Y. Zhao, Y. Wang, X. Zhang, X. Mateos, Z. Pan, P. Loiko, W. Zhou, X. Xu, J. Xu, D. Shen, S. Suomalainen, A. Härkönen, M. Guina, U. Griebner, and V. Petrov, Opt. Lett. **43**, 915 (2018).
5. Y. Zhao, Y. Wang, W. Chen, Z. Pan, L. Wang, X. Dai, H. Yuan, Y. Zhang, H. Cai, J. E. Bae, S. Y. Choi, F. Rotermund, P. Loiko, J. M. Serres, X. Mateos, W. Zhou, D. Shen, U. Griebner, and V. Petrov, Opt. Express **27**, 1922 (2019).
6. E. Kifle, P. Loiko, J. R. V. de Aldana, A. Ródenas, S. Y. Choi, F. Rotermund, V. Zakharov, A. Veniaminov, M. Aguiló, F. Díaz, U. Griebner, V. Petrov, and X. Mateos, Phot. Res. **6**, 971 (2018).
7. C. V. Ruiz Madroñero, X. Mateos, P. Loiko, V. Petrov, U. Griebner, M. Aguiló, and F. Díaz, Laser Phys. Lett. **13**, 095801 (2016).
8. P. Loiko, R. Soulard, G. Brasse, J.-L. Doulan, A. Braud, A. Tyazhev, A. Hideur, and P. Camy, Opt. Lett. **43**, 4341 (2018).
9. D. G. Lancaster, S. Gross, H. Ebendorff-Heidepriem, A. Fuerbach, M. J. Withford, and T. M. Monro, Opt. Lett. **37**, 996 (2012).
10. Y. L. Kalachev, V. A. Mikhailov, V. V. Podreshetnikov, and I. A. Shcherbakov, Quantum Electron. **40**, 296 (2010).
11. P. Loiko, R. Thouroude, R. Soulard, L. Guillemot, G. Brasse, J.-L. Doualan, B. Guichardaz, A. Braud, A. Hideur, M. Laroche, H. Gilles, and P. Camy, Opt. Lett. **44**, 3010 (2019).
12. J.M. Serres, P. Loiko, X. Mateos, V. Jambunathan, K. Yumashev, U. Griebner, V. Petrov, M. Aguiló, and F. Díaz, Laser Phys. Lett. **13**, 025801 (2016).

References

1. G. L. Bourdet and G. Lescroart, "Theoretical modeling and design of a Tm, Ho:$YLiF_4$ microchip laser," Appl. Opt. **38**(15), 3275-3281 (1999).
2. P. Loiko, J.M. Serres, X. Mateos, K. Yumashev, N. Kuleshov, V. Petrov, U. Griebner, M. Aguiló, and F. Díaz, "Microchip laser operation of Tm,Ho:$KLu(WO_4)_2$ crystal," Opt. Express **22**(23), 27976-27984 (2014).
3. B. M. Walsh, N. P. Barnes, and B. Di Bartolo, "The temperature dependence of energy transfer between the Tm $^3F_4$ and Ho $^5I_7$ manifolds of Tm-sensitized Ho luminescence in YAG and YLF," J. Lumin. **90**(1-2), 39-48 (2000).
4. Y. Zhao, Y. Wang, X. Zhang, X. Mateos, Z. Pan, P. Loiko, W. Zhou, X. Xu, J. Xu, D. Shen, S. Suomalainen, A. Härkönen, M. Guina, U. Griebner, and V. Petrov, "87-fs mode-locked Tm,Ho:$CaYAlO_4$ laser at ~2043 nm," Opt. Lett. **43**(4), 915-918 (2018).
5. Y. Zhao, Y. Wang, W. Chen, Z. Pan, L. Wang, X. Dai, H. Yuan, Y. Zhang, H. Cai, J. E. Bae, S. Y. Choi, F. Rotermund, P. Loiko, J. M. Serres, X. Mateos, W. Zhou, D. Shen, U. Griebner, and V. Petrov, "67-fs pulse generation from a mode-locked Tm,Ho:CLNGG laser at 2083 nm," Opt. Express **27**(3), 1922-1928 (2019).
6. E. Kifle, P. Loiko, J. R. V. de Aldana, A. Ródenas, S. Y. Choi, F. Rotermund, V. Zakharov, A. Veniaminov, M. Aguiló, F. Díaz, U. Griebner, V. Petrov, and X. Mateos, "Passively Q-switched fs-laser-written thulium waveguide laser based on evanescent field interaction with carbon nanotubes," Phot. Res. **6**(10), 971-980 (2018).
7. C.V. Ruiz Madroñero, X. Mateos, P. Loiko, V. Petrov, U. Griebner, M. Aguiló, and F. Díaz, "Tm,Ho:$KY(WO_4)_2$ planar waveguide laser," Laser Phys. Lett. **13**(9), 095801-1–6 (2016).
8. P. Loiko, R. Soulard, G. Brasse, J.-L. Doulan, A. Braud, A. Tyazhev, A. Hideur, and P. Camy, "Tm,Ho:$LiYF_4$ planar waveguide laser at 2.05 μm," Opt. Lett. **43**(18), 4341-4344 (2018).
9. D. G. Lancaster, S. Gross, H. Ebendorff-Heidepriem, A. Fuerbach, M. J. Withford, and T. M. Monro, "2.1 μm waveguide laser fabricated by femtosecond laser direct-writing in Ho^{3+}, Tm^{3+}:ZBLAN glass," Opt. Lett. **37**(6), 996-998 (2012).
10. Y. L. Kalachev, V. A. Mikhailov, V. V. Podreshetnikov, and I. A. Shcherbakov, "Study of a Tm:Ho:YLF laser pumped by a Raman shifted erbium-doped fibre laser at 1678 nm," Quantum Electron. **40**(4), 296-300 (2010).
11. P. Loiko, R. Thouroude, R. Soulard, L. Guillemot, G. Brasse, J.-L. Doualan, B. Guichardaz, A. Braud, A. Hideur, M. Laroche, H. Gilles, and P. Camy, "In-band pumping of Tm:$LiYF_4$ channel waveguide: A power scaling strategy for ~2 μm waveguide lasers," Opt. Lett. **44**(12), 3010-3013 (2019).
12. J.M. Serres, P. Loiko, X. Mateos, V. Jambunathan, K. Yumashev, U. Griebner, V. Petrov, M. Aguiló, and F. Díaz, "Q-switching of Tm,Ho:$KLu(WO_4)_2$ microchip laser by a graphene-based saturable absorber," Laser Phys. Lett. **13**(2), 025801-1-5 (2016).